A Laboratory Model of Cooling over the Continental Shelf *

J. A. WHITEHEAD

Woods Hole Oceanographic Institution, Woods Hole, Massachusetts

(Manuscript received 27 July 1992, in final form 29 March 1993)

ABSTRACT

A laboratory experiment is conducted where hot water is cooled by exposure to air in a cylindrical rotating tank with a flat shallow outer "continental shelf" region next to a sloping "continental slope" bottom and a flat "deep ocean" center. It is taken to be a model of wintertime cooling over a continental shelf. The flow on the shelf consists of cellular convection cells descending from the top cooled surface into a region with very complicated baroclinic eddies. Extremely pronounced fronts are found at the shelf break and over the slope. Associated with these are sizable geostrophic currents along the shelf and over shelf break contours. Eddies are particularly energetic there. Cooling rate of the hot water is determined and compared with the temperature difference between the continental shelf and deep ocean. The results are compared with scaling arguments to produce an empirical best-fit formula that agrees with the experiment over a wide range of experimental parameters. A relatively straight trend of the data causes a good collapse to a regression line for all experiments. These experiments have the same range of governing dimensionless numbers as actual ocean continental shelves in some Arctic regions. Therefore, this formula can be used to estimate how much temperature decrease between shelf and offshore will be produced by a given cooling rate by wintertime cooling over continental shelves. The formula is also generalized to include brine rejection by ice formation. It is found that for a given ocean cooling rate, shelf water will be made denser by brine rejection than by thermal contraction. Estimates of water density increase implied by these formulas are useful to determine optimum conditions for deep-water formation in polar regions. For instance, shelves longer than the length scale $0.09fW^{5/3}/B^{1/3}$ (where f is the Coriolis parameter, W is shelf width, and B is buoyancy flux) will produce denser water than shorter shelves. In all cases, effects of earth rotation are very important, and the water will be much denser than if the fluid was not rotating.

1. Introduction

The densest water in the ocean is found at the bottom of polar seas. To acquire that density, surface water experienced either temperature decrease through cooling or salinity increase by evaporation or ice formation. A recent collection of both oceanographic and modeling studies of the cooling and sinking is contained in Chu and Gascard (1991). There are two classes of sinking regions—deep regions and continental shelves. An excellent example of a deep region is found during the winter in the gyre of the Greenland Sea south of the Fram Strait. The surface mixed layer of the ocean penetrates deeply into the stratified water lying below the mixed layer. The deepened mixed layer in the gyre is surrounded by water outside the gyre without such a deepened layer. The entire parcel of dense mixed water presumably sinks by widening at the bottom and narrowing at the top, where light water flows inward. After a suitable time interval, the surrounding lighter water will completely cover the parcel of cold dense water. Once the covering process is complete, additional water of that density will not be formed until the entire mixed-layer deepening process is repeated. This may take weeks or years.

Sinking on a continental shelf proceeds in a different way. Water cooled on the shelf accumulates until pools of dense water get large enough to seek channels to the bottom. Water flowing away from the region of formation becomes impeded by fronts with geostrophic flow at right angles to the pressure gradient. Water flowing in to replace the outflow of dense water is also influenced by rotation. The final flux depends on either bathymetric channels, Ekman layer transport, or eddies from cross-frontal instability. Once the dense water crosses the shelf break, it sinks to the bottom along a density current on the continental slope.

The rate at which water sinks away from the surface influences both the density change of the water and the volume of water that has become denser for any given rate of surface cooling. Although this is obvious and sensible, little work has been done to quantify these considerations. Such an attempt is presented here. First, assume that water with temperature T flows into a control volume with flux Q. Within the volume, water

* Woods Hole Oceanographic Institution Contribution Number 8059.

Corresponding author address: Dr. J. A. Whitehead, Department of Physical Oceanography, Woods Hole Oceanographic Institution, Woods Hole, MA 02543.

is cooled by a negative surface heat flux H per unit area over the area A. Also, assume that temperature inside the volume is not changing with time. The water flows out with temperature $T - \Delta T$ but still with volume flux Q. Conservation of energy is

$$HA = \rho c_p Q \Delta T, \quad (1)$$

where ρ is density and c_p is specific heat. Given fixed H and A, which we assume are determined by both air–sea interaction and preconditioning, we assume that in the ocean Q and ΔT are unknown. Therefore, they form a hyperbola when plotted against each other. This simple relation corresponds to an *open system.* The same relation holds for other systems as well. For instance, it is also valid for a *closed system* where water in volume V changes temperature by ΔT over a time τ so that $Q = V/\tau$.

The magnitude of Q in response to some density difference (as represented by ΔT) is determined by the dynamics of the problem under consideration. The dynamics can be represented by a second trajectory in Q and ΔT space. The intersection of this trajectory with the hyperbola given by Eq. (1) determines the values of Q and ΔT that are expected in each case. If the dynamic trajectory intersects the hyperbola at a value of ΔT that is *smaller* than the total temperature difference between top and bottom ocean waters near where the cooling takes place, the water so cooled will not be cold enough and hence dense enough to sink to the bottom. These dynamics lead to water mass formation of intermediate water. Dynamics that produce larger values of ΔT produce deep or bottom water.

Such dynamic processes are governed by convective processes influenced by local conditions such as bottom bathymetry, local stratification, and shear. One process that can hold water close to the surface for long periods of time arises on shallow continental shelves, where denser water must flow tens or possibly even hundreds of kilometers across the shelf before it encounters the shelf break and deeper water. This tendency to accumulate dense water from wintertime cooling is absent on many shelves because they are covered with lower salinity water than the nearby ocean. The "freshness" from continental runoff generally overcomes the tendency for water in shallow seas to become dense by cooling in the winter. An excellent example of this is seen in sections by Beardsley et al. (1985) on the Mid-Atlantic Bight, where low temperatures from wintertime cooling are balanced by low salinity of the onshore shelf water. However, some continental shelves are an exception (e.g., eastern Barents Sea where freshwater runoff is small), and either strong evaporation or vigorous ice formation in conjunction with local currents makes them important candidates for contributing water by sinking to the deep ocean or even to the ocean bottom itself.

In the Arctic Ocean, for example, Smith et al. (1990) review the role of polynyas and leads in bottom water formation in polar regions. Aagaard et al. (1981) estimate that between 2.5 and 5 ($\times 10^6$ m^3 s^{-1}) of water with salinity 34.75 psu and a temperature of -2°C are needed to maintain the Arctic Ocean Intermediate Water. One of the two hypothesized mechanisms is the cooling and salt increase by ice formation of Arctic continental shelf water. The suggested region for dense water formation is the Siberian shelf. The presence of dense water and the possibility of subsequent sinking into the Eurasian basin has also been discussed by Swift et al. (1983), who incorporated convincing radionuclide evidence that shelf water participated in the intermediate water formation process. Midttun (1985) explained the importance of the marginal ice zone in the bottom-water formation process, since near the freezing point ice formation and subsequent brine rejection changes density of water more than thermal contraction. He also showed summertime sections near Novaya Zemlya in the Barents Sea that indicated dense water on shelves and discussed the role of polynyas in forming that water. Martin and Cavalieri (1989) then estimated the contribution from this region by polynyas. Their results imply that there is an insufficient volume of cold dense water produced in the shelf polynyas for the total required amount, although there is enough to supply a substantial portion.

There are also studies in the Antarctic region. Foster and Carmack (1976) showed the importance of the frontal zone that divides shelf water from offshore water in the southern Weddell Sea shelf. Using the observation that salinity change is 0.2 psu and incorporating estimates of ice formation, they estimated volume flux at 2×10^6 m^3 s^{-1}. Bromwich and Kurz (1984) report on the presence of a polynya in western Terra Nova Bay in the Ross Sea and give estimates of cooling between 500 and 800 W m^{-2} from katabatic winds. The depth of the bay reaches 1000 m so that this would be a case of formation over a relatively deep shelf region, but we are not aware of any oceanographic studies that have observed the dense water. Zwally et al. (1985) also discuss the distribution and effects of polynyas and leads in the Antarctic.

It is desirable to develop more quantitative estimates of the relation between temperature difference and volume flux for problems of ocean cooling. This paper reports a laboratory experiment that measures this relation for a model of a long continental shelf. Currently understood theoretical considerations are summarized in section 2. The experiment is described in section 3. A qualitative description of the thermal and velocity structure is given in section 4. The heat flow measurements are described in section 5. Section 6 discusses scaling of the results and some interpretation of the dynamics governing the heat flux. In section 7 the implications and limitations of the results for the oceans are given.

2. Previous theoretical studies

Estimates of the rate of flow off the shelf as a function of temperature difference can be calculated for constant depth shelves using theoretical models of rotating cross-shelf transport like those of Stommel and Leetmaa (1972), Csanady (1976), and Whitehead (1981). In these models, the dense fluid is removed from the shelf by seaward flow in the bottom Ekman layer and replaced by shoreward flow in the top Ekman layer. Estimates of cross-shelf transport rates in the these three studies were made only for a shelf of constant depth. Unfortunately, the flows themselves are baroclinically unstable for most ocean circumstances (Whitehead 1981), so the estimates may be unrealistic. In a computer model by Hsu (1992, personal communication), calculations of cross-shelf transport in the Ekman layer were done for a shelf with sloping bottom. It is not known whether that flow is unstable to three-dimensional disturbances. The flux was determined for a few cases. In all cases some estimate of the rate of transport of the basic states was obtained. It is not known whether these rates are overshadowed by transport from eddies or limited by dynamics of the front at the shelf edge. Another rate-limiting process is found on the front at the edge of the continental shelf. Killworth (1977) explored the structure and the downstream consequences of the front. Models with behavior like the ocean were produced by adopting appropriate mixing coefficients.

An experiment and simple theory was conducted by Sugimoto and Whitehead (1983) for a rotating bay type of shelf. The tank consisted of a shallow rectangular bay bordered on three sides by vertical walls and on the fourth by a steep sloping bottom that connected the bay to a deep offshore basin. The offshore side of the deep basin was a metal wall connected to a thermostatic hot bath. The top surface of the water was in contact with a Plexiglas lid flushed by cold water, so the entire basin was subjected to surface cooling. The heat flow law in the limit of fast rotation was thought to be provided by the geostrophic flow of the currents entering and leaving the shallow bay. The currents lean on the sidewalls that stretch across the model continental shelf from coast to offshore. Experimental verification for the functional form of this law was found but the constant of proportionality was not fully explained. A numerical study of a cooled rectangular bay by Killworth (1974) was comprised of two layers with changing density. The results were plausible, but it was not conducted over a large range of parameters, so parametric results cannot be compared with the above theories.

Studies that ignore rotation apply to smaller estuarine regions. Endoh (1977) constructed a model of cooling of a steplike shelf with both salt and thermal forcing and found the formation of a thermohaline front at the edge of the shelf. Kowalik and Matthews (1983) conducted a numerical study of a nonrotating bay type of shelf. They recovered velocity magnitude of 1 cm s^{-1} and a realistic density distribution, but there was no search through governing parameter space that would allow the results to be applied to other problems. Brocard et al. (1977) and Brocard and Harleman (1980) intended to model flushing in side arms of cooling lakes. In their theoretical formulation the flushing mechanism was expressed using a two-layer formulation where warm surface water flowed into the cooling lake. It then descended by surface cooling in a mixed region beyond a singular point where Froude number $u/(g'h_1)^{1/2}$ equaled a given value and flowed out along the bottom. In this formula, u is velocity of the water into the cooling lake, h_1 is depth of the layer, and g' is gravity g times density difference between the cold water and the warm water, normalized by average density of the water. The speed of the flow was limited by turbulent friction. Laboratory experiments were used to verify the law relating heat flux with the temperature difference between offshore and the lake. There was satisfactory agreement between the law and the observations. A specific formula from this law subject to one simplifying assumption is given in section 6 of this paper.

This formula is very similar to formulas arising from a second group of calculations that ignore friction entirely but limit the speed of the flow by inertia. The theory used for these calculations has many names, such as overmixing (Stommel and Farmer 1952a,b; Bryden and Stommel 1984), lock exchange (Wood (1970), and maximal exchange (Farmer and Armi 1986). Predictions relating heat flux and temperature difference between offshore and the deep region can also be determined using other studies of two-layer critically controlled flows as given, for instance, by Yih (1980) or Armi (1986). In most cases there is approximate agreement between the formulas and laboratory results. These formulas will be used to test the results for experiments at zero rotation rate and will be discussed in more detail in section 6.

3. The experimental apparatus

Our objective is to investigate relations between temperature difference (shelf to offshore) and heat flux for the laboratory equivalent of very long continental shelves. It was desired to eliminate sidewalls from coast to offshore since they were seen by Sugimoto and Whitehead to support cross-shelf geostrophic currents. To accomplish this, an annular geometry was used. A cylindrical tank was fitted with a shallow but wide shelf along its outer perimeter as shown in Fig. 1. The inside radius of this shelf was 52.7 cm and the outside radius was 80.25 cm. Bordering the shelf on the outside was a vertical wall 25-cm high. Bordering it on the inside was a sloping conical bottom with a 45-deg slope that descended to a deep flat bottom of radius 25 cm. The horizontal bottoms of the tank were leveled so that

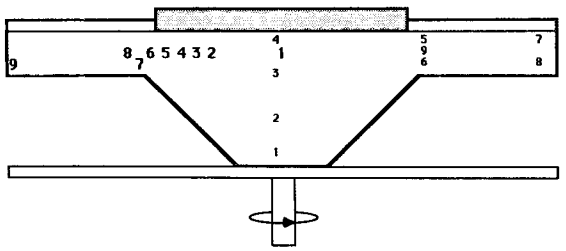

FIG. 1. Sketch of apparatus and layout of thermistors. The thermistor locations shown in small numbers are for the exploratory experiments, and those shown by larger numbers are for the final experiments. The gray cover on the top center is Styrofoam. The tank was insulated on the sides and bottom.

depths were level to better than 2 mm everywhere. The outside of the tank was covered by one-inch foam thermal insulation to retard conductive heat transfer to the room through the walls and bottom of the tank. The tank was mounted on the two-meter turntable at the Coastal Research Center of Woods Hole Oceanographic Institution. This turntable is capable of angular rotation speeds: $2\Omega = f$ of 0.008 to 1 s^{-1}.

To cool the top of the water, the tank was filled with warm water with a temperature of approximately 45°C, which was exposed to air at room temperature. A Styrofoam lid 0.8-cm thick was placed over the central 50-cm radius of the tank to localize the cooling to the shelf region and to eliminate a large offshore current. The current was a consequence of the cylindrical geometry and was felt to be oceanographically unrealistic. Estimates of heat flux were obtained by recording the rate of temperature change and multiplying it by volume of the tank, specific heat of water, and density of water. Calculations indicate that these are as accurate as those obtained by Sugimoto and Whitehead with the Plexiglas lid. The estimates were then compared with recordings of temperature difference between shelf and offshore to produce an empirical relation between heat flux and temperature difference that might apply to cross-shelf heat flow estimates on continental shelves.

4. Structure of the temperature and flow field

The purpose of this section is to give a qualitative and crude quantitative image of the temperature and flow field. (Those interested in the question of heat flux and temperature difference can skip to section 5.) A typical temperature section along a radial line from the outer wall to the center is shown in Fig. 2. In this experimental run there was no insulation on the top surface, so surface cooling was constant everywhere. Depth of the water on the shelf was 10 cm, the rotation rate $f = 1.000$ s^{-1}, and the experiment had been running for about three hours when the section was taken. One can consult figures showing evolution of the temperature field in the following sections to see that it is likely that the temperature field had become quasi-steady after about two hours. The data were acquired by thermistor readings at eight vertical lines (stations) at distances from the outer wall of 0, 10, 20, 30, 35, 40, 60, and 80 cm. Readings were taken at depths of 0, 2, 4, 6, 8, 10, 15, 20, 25, 30, and 35 cm or until the bottom was touched.

Near the center of the tank, Fig. 2 reveals there is a large region of water with temperature above 32°C. The temperature decreases only slightly with depth except for a region a few centimeters off the bottom where a sharper decrease is found. Temperature also gradually decreases as one moves toward the shelf at all levels. This central region has the lowest temperature gradients of anywhere, and the isotherms are bowl shaped. Over the sloping region, a greater temperature gradient roughly 10 cm above the slope indicates a shelf front. Dye was injected at two levels in this region near the break to get a crude measurement of the speed of the mean alongshelf currents. There is an extremely strong baroclinic shear, with water flowing toward the viewer at a speed of about 0.1 cm s^{-1} near the bottom and away from the viewer at a speed of about 0.5 cm s^{-1} at the top. Evidence of many eddies around and within this front was seen in the dye trajectories. This front is one of the most important features of both the flow and thermal structure in the experiment. Over the flat shelf there is a tilt of isotherms like over the slope, but the isotherms are farther apart. There was a movement of injected dye away from the viewer with a speed of about 0.05 cm s^{-1}.

These velocities are consistent with a thermal wind balance using

$$f\frac{\partial v}{\partial z} = \frac{-g}{\rho}\frac{\partial \rho}{\partial x}, \tag{2}$$

where z is the vertical direction, x increases from left to right in Fig. 2, and v is positive away from us. For the frontal region, using $\rho = \rho_0(1 - \alpha T)$, where $\alpha = 2 \times 10^{-4}$ °C^{-1} and taking both x and z scales to be 10 cm, we estimate from Fig. 2 that there is a lateral temperature change of 2°C over 10 cm in the front

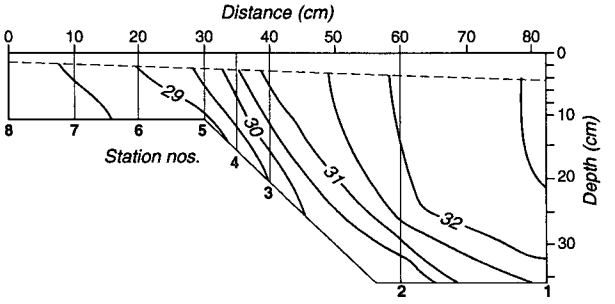

FIG. 2. A temperature section along a radial line from the coast (left) to the center (right) after cooling for about three hours. Isotherms are shown in intervals of 0.5°C. The top mixed layer is above the dashed line.

region. This gives an alongshelf velocity change of 0.4 cm s^{-1} over a vertical distance of 10 cm, a value somewhat lower than our observed velocity change of 0.6 cm s^{-1} between the top of the shelf break and the bottom. On the shelf a 0.4°C temperature change in 10 cm is reasonable. This gives a predicted vertical change of velocity of 0.08 cm s^{-1}. Assuming velocity is zero at the bottom boundary of the shelf, we predict 0.08 cm s^{-1} at the very top of the 10-cm-deep water. This is roughly the 0.05 cm s^{-1} estimated from the dye, which was conveyed up and down by convection and geostrophic turbulence so that it did not apply to any particular depth.

For most runs the flow was very irregular, characterized by baroclinic eddies superimposed on the drifts estimated above. Starting from offshore, the density current descended to the bottom of the tank where it tended to break up into irregular blobs. Above these blobs was intense cyclonic eddy activity, similar to that described by Whitehead et al. (1990). The cyclones were so strong that dimples were often easily seen on the top free surface of the water. On the shelf itself there were two eddy scales as shown in Fig. 3. The larger of the two consisted of circular conical blobs of cold water that had accumulated from surface cooling. These blobs were surrounded by wisps of dye in Fig. 3. They tended to move around. It was not possible to identify individual blobs for a long enough time to see whether they gradually got to the shelf break and fell off the edge before changing their shape or whether instead they changed many times before the cold water found its way to the edge of the break. The second scale was from convection cells. These consisted of inverted plumes of cold surface water sinking to the bottom. They are revealed as white circular holes in the dye in Fig. 3. This figure was taken from an experiment with the relatively rapid rotation rate of $f = 1.000\ s^{-1}$. Although the two scales seem similar in size, for slow rotation rates the baroclinic eddy scale was much larger than the convection scale. The overall pattern of flows is similar to that described in Sugimoto and Whitehead. When the internal Rossby radius of deformation was as large as the width of the shelf, there tended to be large baroclinic eddies on the shelf. These possessed patches of convection cells in preferential regions. Around these eddies, sinuous jetlike fronts often appeared to wander from the inner wall to over the shelf break. They are similar to those seen in annulus experiments (Fultz 1961; Hide and Mason 1975). The dye revealed that fronts (both on the shelf and over the shelf break) generally penetrated from surface to bottom, so the eddies had a strong barotropic component in addition to their baroclinic nature. Only when rotation was very slow did the eddies of dense water appear to be bottom trapped and surface water top trapped. The measurement of eddy scale was beyond the scope of this project, so no information is available as to the scale of eddies as a function of the experimental parameters.

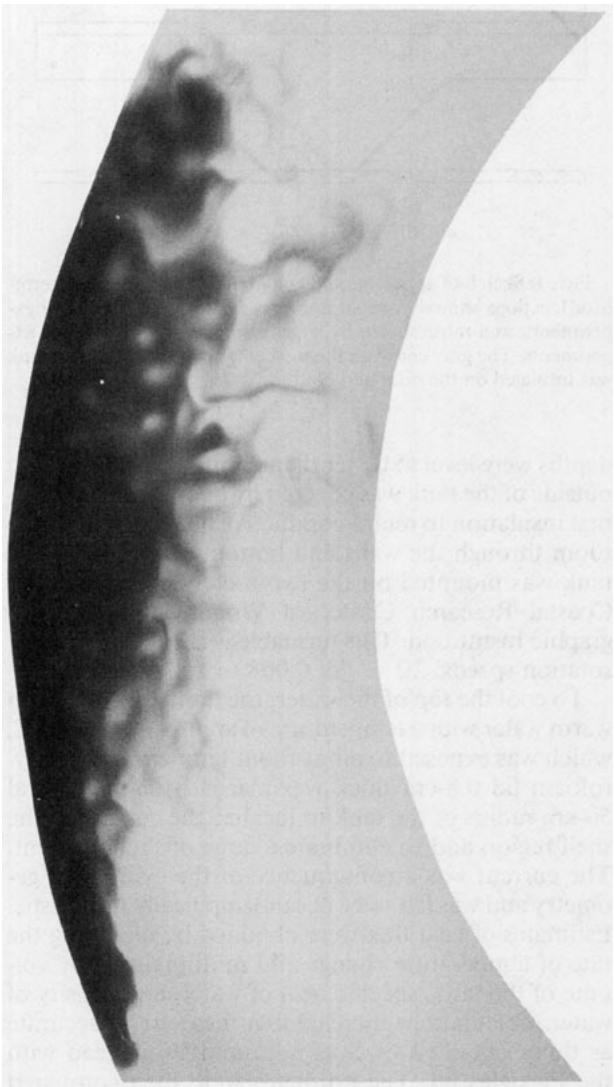

FIG. 3. A photograph of a pool of dye lying on the bottom of the laboratory model of the continental shelf. The wisps of dye extending to the right surround circular baroclinic eddies that consist of conical blobs of clear cold water. The holes in the dye denote the sinking centers of convection cells.

Figure 4 shows streak photographs of surface flow in experiments with no Styrofoam lid. In the central "deep ocean" region is a circulation that is rapid and relatively steady. Standing in the laboratory, we saw that the flow had almost no rotation. Thus, in the rotating frame the flow is anticyclonic. This circulation arises because of the upwelling of warm water in the deep basin since it is being replenished from below by cooled water from the shelf and is flowing onto the shelf at the surface to replace that cooled water. This very rapid offshore current is undesirable since oceans do not have them (it is a consequence of the smallness

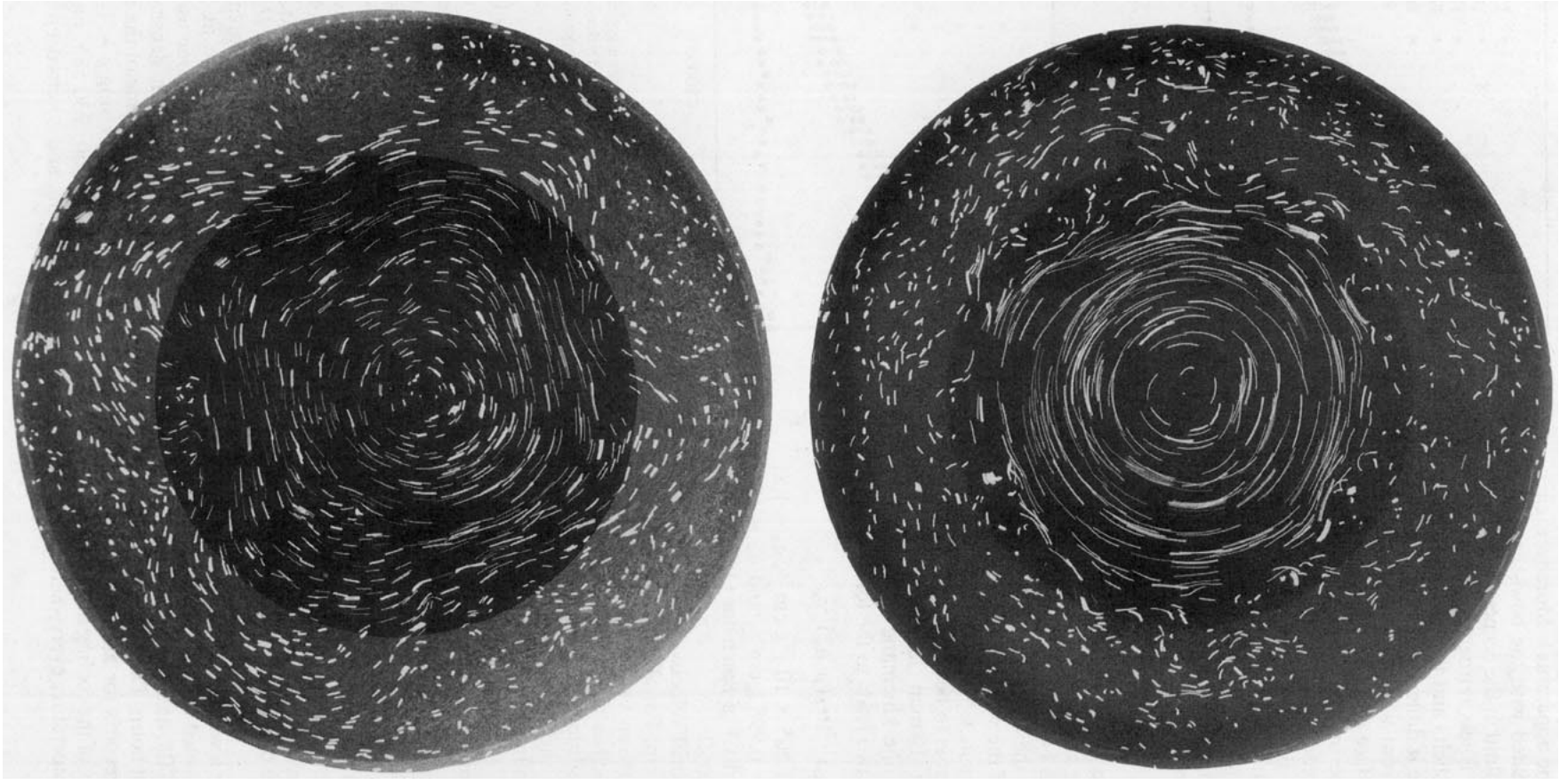

FIG. 4. Streak photographs with a 4-s time exposure of surface pellets for the rotation rates of $f = 0.500$ (left) and 0.250 (right). The large anticyclonic circulation over the central deep regions is the most striking flow. Covers were devised to eliminate that flow since it is not representative of the ocean. Outside of the shelf break is a strong front where velocity decreases sharply and eddies are present. In some cases such as on the left, the eddies are associated with significant meandering of the offshore front, but in other cases there is little correlation between the eddies and the front location. Eddies also lie on the shelf and appear to be responsible for some of the cross-shelf transport.

of the deep basin of the apparatus). Moreover, circulation is clearly associated with the bowl-shaped isotherms in Fig. 2 since fluid in the deeper regions of the central "deep ocean" is less retrograde (because it is not flowing onto the shelf) and thus is less divergent. These isotherms made it difficult to decide where the offshore edge of the front was. There is also a sharp lateral shear in the surface region 5–15 cm offshore of the shelf break. At the inshore side of the shear the flow has considerable eddy activity, which is also seen farther onshore. Over the shelf itself there is a much smaller velocity, which is again retrograde.

Some of the above flow may be driven by air drag. Consider that drag of air D_a on the surface of the water at radius r is approximately

$$D_a = \mu_a \Omega r / d_{ea}, \tag{3}$$

where μ_a is the viscosity of the air, Ωr is the differential speed between the air and the water, and d_{ea} is the Ekman layer thickness $[=(\nu_a/f)^{1/2}]$, where ν_a is the kinematic viscosity of the air. This equals the Ekman drag on the bottom of the water on the shelf of magnitude $\mu_w U/d_{ew}$, where μ_w is the viscosity of water, U is the drift velocity that is to be calculated, and d_{ew} is the thickness of the Ekman layer of the water $(\nu_w/f)^{1/2}$ where ν_w is the kinematic viscosity of the water. Equating these two leads to the formula

$$U = (\rho_a \mu_a)^{1/2} \Omega r / (\rho_w \mu_w)^{1/2}; \tag{4}$$

using the values $\rho_a = 1.205 \times 10^{-3}$ g cm^{-3}, $\mu_a = 1.81 \times 10^{-4}$ g cm^{-1} s, $\rho_w = 0.998$ g cm^{-3}, and $\mu_w = 10^{-2}$ g cm^{-1} s [from appendix I of Batchelor (1967)], this is approximately $=0.005\Omega r$.

Equation (4) gives drift velocity of 0.13 cm s^{-1} for $f = 1$ s^{-1} and $r = 50$ cm. For all the observations in this study, this wind-driven velocity is much smaller than the observed velocities at the front near the shelf break. However, it is a little larger than the magnitude of the velocity on the shelf, and the drift current on the shelf is probably influenced by air drag.

5. Heat flow measurements

To calculate heat flux, use was made of the transient nature of the experiment. Exploratory runs were conducted with thermistor locations shown by small numbers and final runs had locations shown by large numbers in Fig. 2. Depth of water on the shelf was either 5, 10, or 20 cm. Details of the development of the observation scheme are discussed in a technical report (Whitehead 1993).

To obtain data over a wide range of rotation rates, experiments were conducted for $f = 1$, 0.5, 0.25, 0.125, 0.063, 0.032, 0.016, 0.008, and 0 s^{-1}. Each run lasted for approximately eight hours. Data were recorded every 15 minutes. The records for all nine thermistors were digitized, so a view of the cooling in all the regions could be obtained. Temperature everywhere exhibited

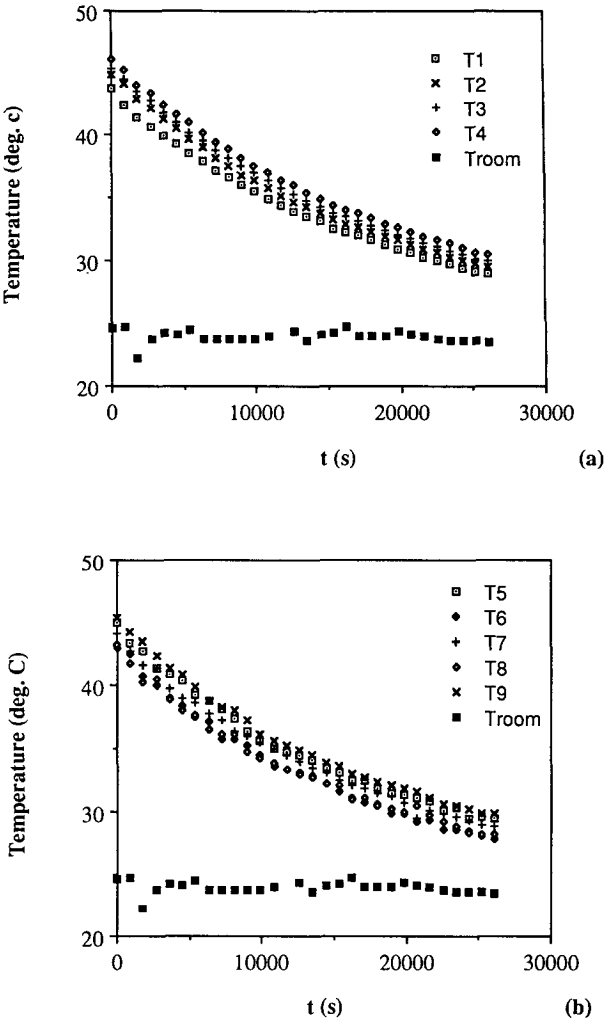

FIG. 5. Temperature as a function of time for a typical experiment. For the preliminary locations shown in Fig. 2, Tn denotes the thermistors: (a) centerline temperatures; (b) shelf temperatures.

almost the same cooling curve. Figures 5a,b show typical records of all nine thermistors in the initial configuration as their temperature slowly decreases during an experiment. The gradual change of the mean temperature with time is obvious. The records appear to exhibit exponential cooling in some cases; unfortunately, not all cooling curves were close enough to exponential to use the characteristics of such behavior for the analysis of the experimental results.

The heat flow (henceforth to be called H_n) from the shelf to the deep basin across the shelf break was estimated from the data of temperature at location n (henceforth to be called T_n) versus time using the formula $H_n = \rho c_p V \partial T_n/\partial t$, where ρ is density of water, c_p is heat capacity, and V is volume of the basin from the shelf break to the center. Using $\rho = 1$ g cm^{-3}; $c_p = 1$ cal/g °C; $V = 186\,960$, 230 585, and 317 835 cm^3 for the 5-cm, 10-cm, and 20-cm deep containers,

respectively, and approximating $\partial T_n/\partial t = \delta T_n/900$ where δT_n is the change in temperature in 900 seconds, the formula for heat flow becomes

$$H_n = C_0 \delta T_n \text{ cal s}^{-1}, \quad (5)$$

where the constant C_0 = 207.73, 256.19, and 353.14 cal/s °C is defined for the three depths. This calculation to estimate heat flux was performed on the entire set of readings of an individual thermistor for the duration of the experiment. Since the time derivative was found using the exact differences between sequential readings, the estimates of cooling versus time were much more irregular than the original temperature records. Thus, the heat flux data were smoothed with a three-point running mean to restore the heat flow data to the smoothness of the original temperature series as a function of time. Figure 6 shows heat flow calculated as a function of time. The numbers exhibited scatter of roughly 50% around a mean value, with a trend toward lower values with time.

Besides being used for the heat flow estimate, the array was also used to determine a typical temperature difference between the shelf and offshore. Figure 6 also shows readings of this difference between two locations with time. As with the heat flow estimate, they exhibited scatter of roughly 50% around a mean value, with a trend toward lower values with time.

Experiments were conducted with two different insulating lids that covered the deep part of the tank. The purpose of the lids was primarily to localize the cooling to only the shelf and thereby to increase accuracy of estimates of heat flow from shelf to offshore. Secondarily, the lids were meant to decrease the intensity of the bowl-shaped isotherms in the deep basin that confused the location of the outer edge of the front. One lid was the Styrofoam cover over the deep basin already described. The other lid was identical to the first but it also had eight radial flow baffles spaced every 45° underneath. These were made of a perforated aluminum sheet, 15 cm deep and extended from the center to a line 5 cm above the shelf slope; they eliminated the large bowl-shaped isotherms in the deep water that were associated with anticyclonic circulation from upwelling in the deep portion of the tank. This made the offshore water stagnant (or at least with a velocity smaller than the shelf flushing velocities studied here) and therefore more like a typical ocean. The baffles also conducted heat vertically so that isothermal water covered the top 15 cm. They did not, however, eliminate the front over the shelf break, which by virtue of its persistence—even with the baffles—was found to be a major percentage of the overall shelf to offshore temperature drop.

The final thermistor array was designed to produce a more accurate picture of the offshore front (Fig. 2). The considerations in Whitehead and Frazel (1993) resulted in using data from thermistors in the new locations 4 and 9 to calculate two values of heat flux, and using the differences between locations 4–9 and 5–9 (henceforth the difference between location n and T_9 will be called D_n) to give two estimates of temperature difference between "shelf and ocean." Choice of these locations resulted from the recognition that more than 50% of the shelf to offshore temperature change happened at the offshore front. This is illustrated in the temperature records shown in Fig. 7. This is also illustrated in Fig. 8, which shows that the data with a baffled experiment are almost identical to those without the baffle. Finally, to eliminate some of the scatter shown in Fig. 6, groups of nine consecutive readings were averaged. Since each experiment had roughly 28 intervals of 15 minutes each over the 8-hour period, this yielded three independent values of temperature difference and heat flux for each data string. Since two measurements were made of heat flux and two of temperature difference, each run resulted in 12 numbers.

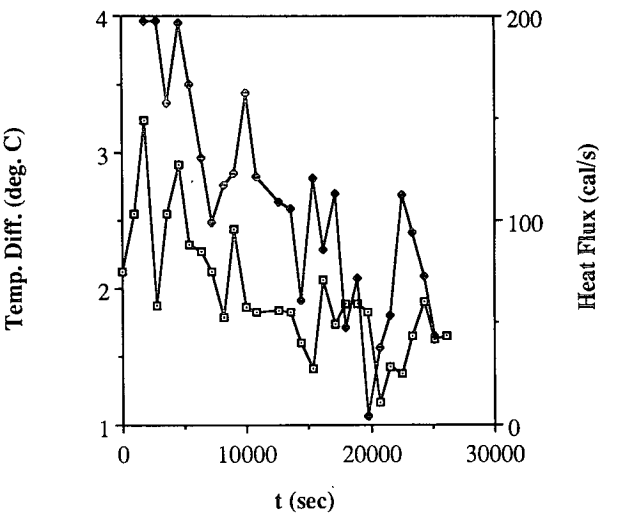

FIG. 6. Measurements in the preliminary experiments of heat flow (solid dots) at location 4 with time and temperature difference between locations 8 and 9 (open squares) with time. Shelf depth h = 5 cm, f = 1.000 s^{-1}.

The data of heat flux versus for D_4 are shown in Fig. 9 for all the rotation rates that were used and for fluid depths of 5 cm, 10 cm (using both baffled and nonbaffled lids), and 20 cm (with a nonbaffled lid). Clearly, temperature differences systematically increase both with increasing heat flow and with greater rotation rate. This is half the dataset. The figures for D_5 are similar to Fig. 9 except that values of temperature were a few percent smaller, so they were not shown. Thus, the absolute value of temperature difference depends on position of the thermistor with respect to the offshore front, but the effect is less than 20% as big as that from changing rotation or fluid depth. Tabulated values and more detailed figures are given in Whitehead and Frazel (1993).

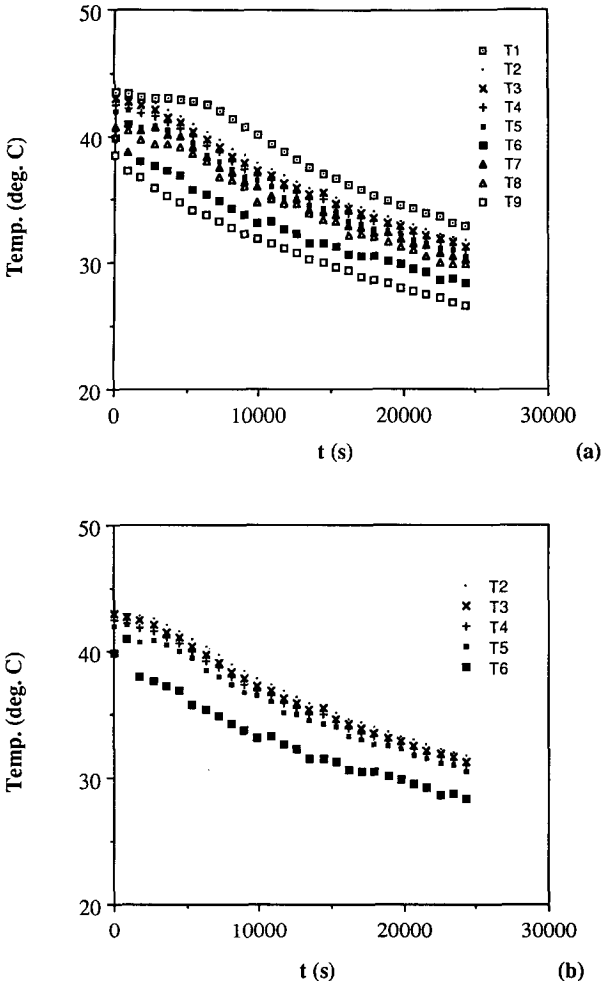

FIG. 7. Temperature versus time for final thermistor placement: (a) All 9 thermistors and (b) thermistors 2 through 6, which lie offshore of the front and maintain close to the same value in comparison to thermistor 9. Shelf depth $h = 5$ cm, $f = 1.000\ s^{-1}$.

It was not obvious how to further analyze the data. Fits to power laws were attempted without useful results. Slopes were found for all data but there was wide scatter between values of slope and the information was of limited value. However, there were some clear trends. First, at rotation rates of roughly 0.032 and less the heat flux as a function of temperature difference approached a log–log power law of 3/2. Second, the fastest rotation rates had a clearly greater power law, possibly up to a power of 3, although scatter is great. These trends were visible both with 10-cm and 20-cm experiments.

A better view was found by first noting that all results had heat flow of approximately 100 cal s^{-1} for the first time interval. Assuming that these results have fixed heat flow, temperature difference at the first time interval can be plotted as a function of f. An example is shown in Fig. 10. It illustrates the effect of rotation on the temperature difference for fixed heat flow. At low and zero rates of rotation as shown to the left, temperature difference has a constant value that is unaffected by rotation. For approximately $f > 0.1\ s^{-1}$, temperature difference increases with f. At the largest value, the slope of temperature difference with f gets close to 1 on a log–log plot.

Inspection of all the data in Fig. 9 revealed that there was consistency with the notion that temperature difference is inversely proportional to depth h, proportional to heat flux to the 2/3 power for low rotation, to the 1/3 power law for fast rotation, and may be approaching a power law of f^1 for fast rotation. Motivated by this, a test was developed to determine whether heat flux data can be used to predict a temperature difference (henceforth called ΔT_h) by the relation

$$\Delta T_h = \frac{c_1(H_n^{2/3})}{h} + \frac{c_2 f(H_n^{1/3})}{h}. \qquad (6)$$

Theoretical justification for the values of the two exponents in Eq. (6) will be discussed in the next section. Values of c_1 were found by least-squares fit for each individual series of runs with the same depth, so that the three values of temperature at zero rotation agree with ΔT_h. Values of c_1 were 0.186 for both D_4 and D_5 with 5-cm depth, 0.18 for both D_4 and D_5 for the baffled cases with 10-cm depth, 0.21 for D_4 and 0.22 for D_5 for the nonbaffled cases with 10-cm depth, and 0.08 for both D_4 and D_5 with 20-cm depth. Note that the values for the first six cases are close to 0.2. In contrast, the experiment with 20-cm depth had a significantly different constant of $c_2 = 0.08$. However, for that depth the ratio of width to depth is 1.5, which is small. Moreover, most of the runs were in the rapidly rotating limit, so we believe the coefficient value of 0.08 is less well established than the others. The value $c_2 = 5$ fits all data nicely.

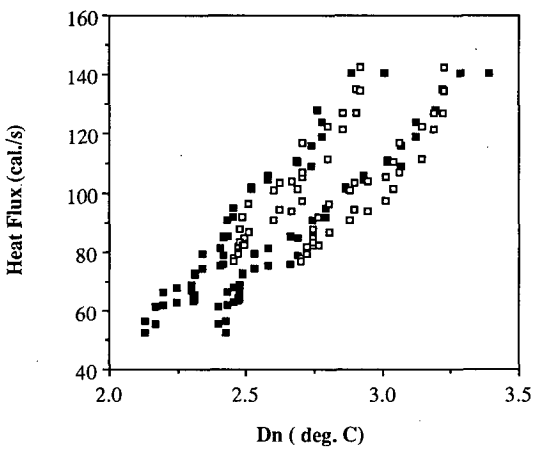

FIG. 8. Heat flux versus D_4 (right-hand cluster) and D_5 (left-hand cluster) for the baffled results (open squares) and nonbaffled results (solid squares).

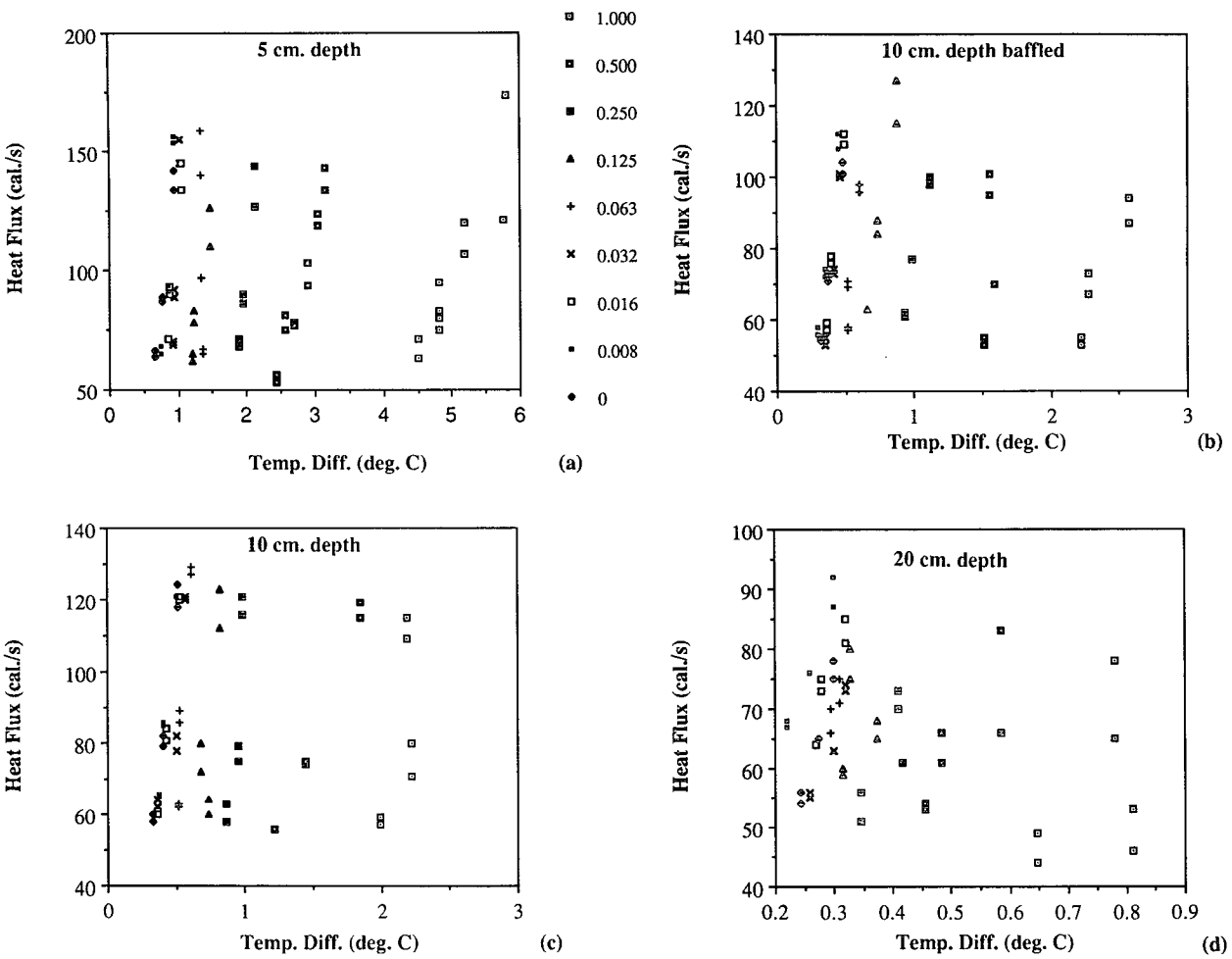

FIG. 9. Heat flux versus temperature difference D_4 for all experiments: (a) 5 cm deep, (b) 10 cm with a baffled lid, (c) 10 cm without a baffled lid, and (d) 20 cm deep. The legend on the right of (a) gives the symbol for each value of rotation f. It is clear that above a certain value of f, temperature difference increases with rotation rate. For all values of f, temperature difference decreases with fluid depth. There is also a weak increase of temperature difference with heat flux. A figure like this for D_5 is very similar except the temperature values are a few percent smaller.

Using Eq. (6), values of ΔT_h were calculated using $c_1 = 0.2$, $c_2 = 5$, and values of H_n, f, and h for each run. These are plotted against D_4 and D_5 in Fig. 11a and as log–log plots in Figs. 11b,c. All reveal a linear relation between the prediction and measurement, so there is surprisingly close agreement between Eq. (6) and the measured temperature difference. The correlation coefficients are more than 0.99, and the slope of the log–log best fit is within 1% of 1.0. In Fig. 11b the two values of D_4 and D_5 are visible as two elongated trends in the data that are offset by less than 20% over a range of more than a factor of 10. This implies that the choice of the exact location of the thermistor offshore of the front is not central to this comparison, since the offset is small compared to the span of the entire results. Figure 11c shows only the D_4 data but each depth has different symbols. It reveals that the 5- and 10-cm results lie along the same line and show considerable overlap, but the 20-cm runs have slightly bigger values of ΔT_h.

To demonstrate that each of the terms in Eq. (6) is insufficient alone, Fig. 12 shows the values of each of the two terms (along with their sum) in comparison with the measured value of temperature. This calculation is done for the 10-cm-deep experiments. It is clear that neither term alone has satisfactory comparison with the measured data over the entire range of rotation rates.

Equation (6) almost collapses the data to a line over the entire range of rotation rates, for all three values of h used, and over a range of a factor of 2 for heat flux. The data with depths of 5 and 10 cm form the best trend that lends strong confirmation to Eq. (6). The data for 20-cm overlap the left-hand end of the dataset but alone would not be consistent with a slope of one. Although the value of the constant c_1 for 20

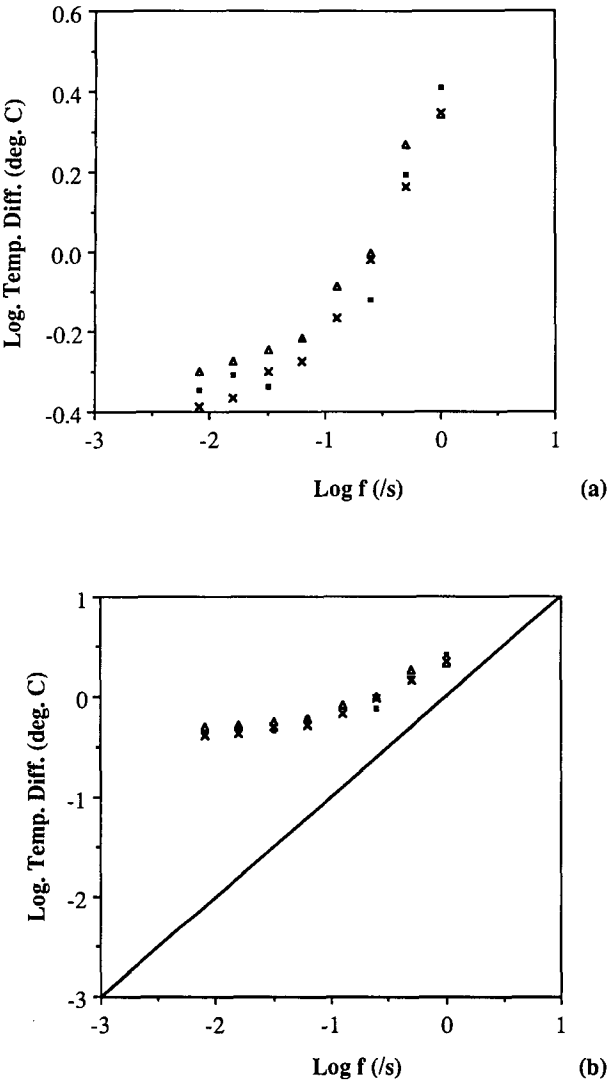

FIG. 10. Temperature difference versus rotation rate for experiments with heat flux of approximately 100 cal s^{-1} and depth of 10 cm. The triangles identify nonbaffled experimental data, the squares indicate baffled data, and the x shows the middle heat flux reading from the nonbaffled experiment. (a) Close-up of the result in log-log space. (b) The same data compared to a line with a slope of 1.

cm was less than half the value for the other depths, this fit was not strongly effected for c_1 over most of the range. Therefore, in view of the wide range of rotation rates, depths, and heat fluxes, and the small aspect ratio for the 20-cm data, it seems that Eq. (6) agrees with the data quite well. This is the principal result of the experiment.

6. Scaling of the results

In this section, the theoretical considerations that are responsible for the scalings that were selected in the last section are reviewed, and then Eq. (6) is converted into a more physically meaningful formula.

Brocard et al. (1977) and Brocard and Harleman (1980) found agreement with the formula $q_0 = (Bh^4/f_0)^{1/3}$ [their Eq. (28) with $h_0 = 1/2$ and $\alpha = 1$], where $q_0 = v_0 h/2$ is the volume flux per unit length. This reduces to the following relations for density scale g' and velocity scale v_0:

$$g' = B^{2/3} W_s f_0^{1/3} / h^{4/3} \tag{7a}$$

$$v_0 = 2(Bh/f_0)^{1/3}, \tag{7b}$$

where symbol f_0 stands for the friction coefficient that was assigned a value of 0.02, h is shelf depth, W_s is width of the shelf, and B is buoyancy flux per unit area, given for our experiment as

$$B = g\alpha H_n / \rho c_p \pi (r_1^2 - r_2^2), \tag{8}$$

with units length^2/time^3. They applied this to finger lakes rather than continental shelves, but the approximations were two-dimensional, so the results should carry over to shelves. This balance also resembles a frictional balance for a freshwater estuary solved by Long (1975).

A second relation called "overmixing" (Stommel and Farmer 1952a,b) can also be used. The result is derived using inertial hydrodynamics and is very similar to the result for lock exchange flow (Wood 1970) (although some of the physical arguments used to derive the governing equations differ). Using the same notation, density difference and velocity are given by

$$g' \sim (4BW_s)^{2/3}/h \tag{9a}$$

$$v_0 \sim (BW_s)^{1/3}. \tag{9b}$$

The width W_s in (9b) replaces h in (7b), and f_0 is eliminated because the velocity is controlled by inertia here rather than by turbulent drag. The constant of proportionality for velocity that is required to make Eq. (9a) an equality has been the focus of considerable study by Bryden and Kinder (1991), Farmer and Armi (1986), and Yih (1980). It ranges from under 1/4 to 1/2, depending upon geometric details. Velocity is controlled here by inertia rather than turbulent drag.

Equations (7) or (9) constitute two possible balances between density difference and buoyancy flux that are valid for zero rotation. For large rotation rate, we expect that if temperature difference is proportional to Coriolis parameter f and if it is inversely proportional to shelf depth h, dimensional considerations dictate that the temperature difference will be given by

$$g' \sim f(BW_s^4)^{1/3}/h. \tag{10a}$$

This has the form of the extreme right-hand relation in Eq. (6). Velocity scale is

$$v_0 \sim 2B^{2/3}/fW_s^{1/3}. \tag{10b}$$

This is found from Eq. (10a) using the buoyancy flux relation

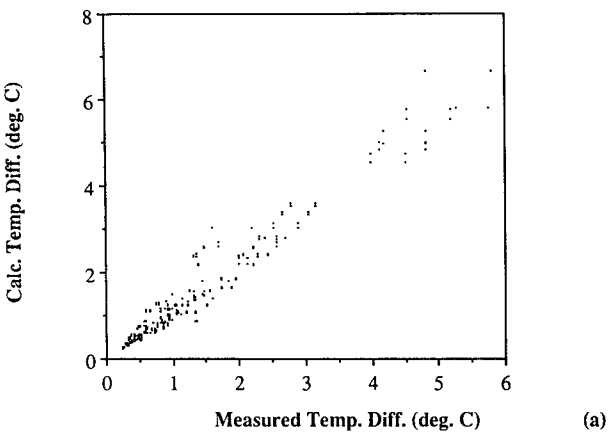

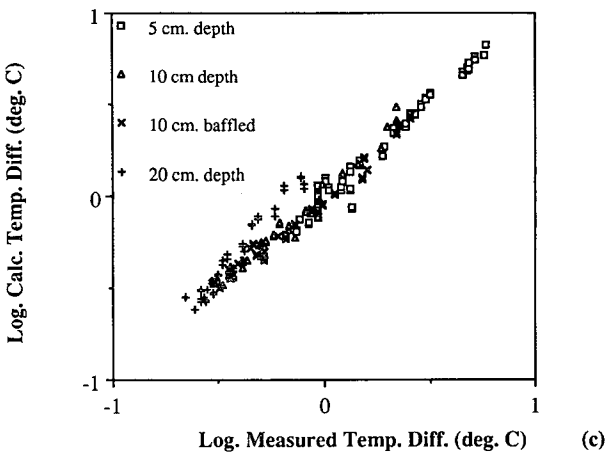

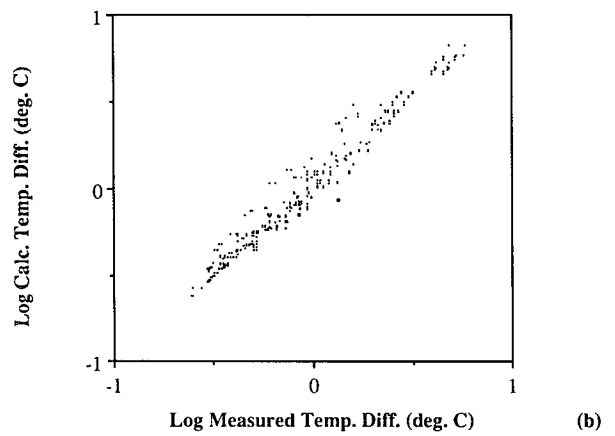

FIG. 11. (a) All measured values of D_4 and D_5 versus ΔT_h; (b) the same in logarithm scale; and (c) the same as (b) but for only D_4 and with each depth denoted by a different symbol.

$$BW_s = g' v_0 h/2. \tag{10c}$$

This relation is comparable to the conservation of energy that was discussed in the Introduction and given in Eq. (1).

These relations can be derived from Eq. (10b) in Whitehead (1981) with surface velocities U, $V = 0$. In the limit of small Ekman number, it reduces to

$$\frac{H_n}{2\pi r_2} = \frac{\rho c_p g^2 \alpha^2 \,\mathrm{Pr}\, d^3 (\partial T/\partial r)^3}{4f^3}, \tag{11a}$$

where Pr is Prandtl number and r is the radius on the shelf. If one assumes that $\partial T/\partial r$ equals temperature difference from shelf to offshore divided by W_s, this reduces to

$$g' = 2f(BW_s^4/\mathrm{Pr})^{1/3}/h, \tag{11b}$$

which is proportional to our Eq. (10a). This theory was produced from the Stommel–Leetmaa solution (Stommel and Leetmaa 1972; Csanady 1976; Whitehead 1981) for flow over a continental shelf with flat bottom where heat flux is provided by flux in the Ekman layers down the temperature gradient. That it should apply in detail to the temperature drop in this problem (which is principally across the front at the shelf break) is not clear. A preliminary interpretation is that the flow on the flat portion of the shelf is baroclinically unstable (Whitehead 1981) and thus transports heat more effectively than the aforementioned law but that at the shelf break the slope stabilizes the flow and requires this Ekman layer mechanism of buoyancy flux through the front. Future work is planned to investigate this interesting possibility.

To produce an equation with the form of Eq. (6), terms in Eqs. (9a) and (10a) were multiplied separately by unknown proportionality constants; then the products were added together. Using the experimentally observed $c_1 = 0.2$ and $c_2 = 5$, with values for the laboratory experiment of $g = 980$ cm s^{-2}, $\alpha = 3 \times 10^{-4}$ °C^{-1}, $\rho = 1.0$ g cm^{-3}, $c_p = 1.0$ cal./°C g, and $W_s = r_1 - r_2$ cm along with Eq. (8), we produce an empirical relation between heat flow H per unit area $[= H_n/\pi(r_1^2 - r_2^2)]$ and temperature difference between shelf and offshore:

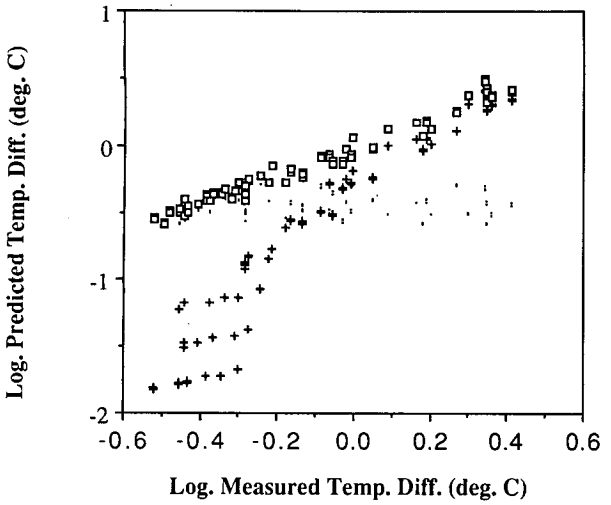

FIG. 12. Measured values of D_4 and D_5 versus predicted values from heat flow measurements. The data shown as very small dots use the zero rotation term $c_1 H_n^{2/3}/h$ for predicted temperature difference. The data shown as small rectangles use the rotation term $c_2 f H_n^{1/3}/h$ for predicted temperature difference. The sum of these two terms corresponds to equation (6) and is shown as open squares. These are included in the data shown in Fig. 11. All data from the 10-cm-deep experiments were used for this figure.

$$\Delta T = \frac{1}{g\alpha h}\left[7.4\left(\frac{g\alpha H W_s}{\rho c_p}\right)^{2/3} + 0.6 f W_s\left(\frac{g\alpha H W_s}{\rho c_p}\right)^{1/3}\right]. \quad (12)$$

This equation is a best fit to the data from the experiments. Both scaling constants differ from their counterparts in the ideal theories. The value 7.4 differs from $4^{2/3}/2$ [from Eq. (9a)] by a factor of 6, and 0.6 differs from 2 [from Eq. (11b)] by a factor of 0.3. The difference is not surprising in view of the significant differences between the ideal, Cartesian, slowly varying laminar theories and the complicated real geometry with turbulent flows and extra stresses.

Note that both viscosity and thermal conductivity have small contributions in the final formulas. It is difficult to be precise about their contribution in any single run through simple scaling. A spindown time scale $d/(\nu_w f)^{1/2}$ ranges from a quite small value of 50 s (for $d = 5$ cm and $f = 1\ s^{-1}$) to values of over hours. However, this scale applies to a homogeneous fluid and might not be important in this experiment. A thermally stratified fluid has a time scale that might be as large as the viscous time scale d^2/ν_w, which ranges from 42 minutes upward. For small rotation, the agreement of the lock-exchange scaling and the disagreement with the turbulent friction scaling of Brocard et al. indicates that friction is not too important. Viscosity could, however, decrease the flux and lead to the fact that the empirical constant is larger in the experiment than in theory. Without doubt, a useful guide concerning friction and diffusivity comes from the fact that the Stommel–Leetmaa solution recovers the same scaling as these laboratory experiments.

7. Implications and limitations of the results

The insertion of test values into Eq. (12) will give some insight into how much temperature deficiency accumulates on a shelf before the cross-shelf exchange prevents the further lowering of the temperature. Taking values of $g = 10\ m\ s^{-2}$, $\alpha = 10^{-4}\ °C^{-1}$, $f = 10^4\ s^{-1}$, a large value of heat flux $H = 1000\ W\ m^{-2}$, $W_s = 100$ km, $\rho = 10^3\ kg\ m^{-3}$, $c_p = 4 \times 10^3\ J\ (kg\ °C)^{-1}$, and $h = 100$ m, Eq. (12) shows that the left-hand (nonrotating, lock-exchange) term gives a temperature decrease of 6.3°C and the right-hand term gives a decrease of 17.5°C. Thus, under these extreme ocean cooling conditions, water becomes roughly three times colder and denser on shelves due to rotational hydrodynamic effects. The two terms add up to a predicted temperature decrease of 23.8°C. This is a huge value and is possible only under extreme conditions of high winds and subzero air temperatures, and of course, nonlinearities in the equation of state would be important. Such conditions would be in existence only for a few days at most. Conditions averaged over a winter, and with greater shelf depths, might be many times smaller. Taking, for example, a value of heat flux four times smaller reduces the nonrotating component to 2.5°C and the rotating one to a value of 11.0 for a total of 13.5°C. Taking a shelf three times deeper as well reduces the nonrotating component to 0.8°C and the rotating one to a value of 4.5°C for a total of 5.3°C.

The volume flux associated with this temperature difference and cooling rate is found from Eq. (1). Flux is linearly proportional to the length Λ of the shelf. Taking $\Lambda = 1000$ km, and a temperature difference of 25°C (a value close to the value 23.8°C found above), we get $Q = 1.3 \times 10^6\ m^3\ s^{-1}$. Aagaard et al. (1981) estimate a magnitude of $2.5 \times 10^6\ m^3\ s^{-1}$ of dense water feeds into the polar basin. This is greater but of the same order of magnitude as our number. However, the agreement with our number is not very significant at this stage since we use arbitrary (and very large) values of cooling rate and ignore salt effects that surely are important.

The results can be put into more general form using reduced gravity $g' = g\alpha\Delta T$ and buoyancy flux $B = g\alpha H/\rho c_p$ in Eq. (12):

$$g'h = 7.4(BW_s)^{2/3} + 0.6 f W_s (BW_s)^{1/3}. \quad (13)$$

The conditions for rotational effects to dominate over nonrotational effects are found by requiring the first term on the right in Eq. (13) to be less than the second. This means that $(BW_s)^{1/3} < 0.08 f W_s$. One could call the parameter group $(B/W_s^2 f^3)$ a heat flux Rossby radius. Note that shelf depth h is not present. Using above values of W_s and f, $H < 21322\ W\ m^{-2}$ for ro-

tational effects to dominate, which is immense, so the criterion is certainly met. However, for a narrower 10-km-wide shelf, $H < 213$ W m^{-2}, which is a reasonable wintertime cooling, so either rotational or nonrotational dynamics might apply. One can also use Eq. (13) in the limit of rapid rotation to show that $(g'h)^{1/2}/f < 0.31 W_s$ for the rotation-dominated case. This states that for rotational effects to dominate, the Rossby radius is less than 0.31 times the width of the shelf. This result is expected and indicates that the theory is sound.

The results can also be compared with the results of Sugimoto and Whitehead (1983) for cooling of a bay. Their results were that $g'h = 2(fBW_sL)^{1/2}$ (approximately, there is a poorly understood constant of proportionality) in the limit of rapid rotation where L is the alongshelf length of the bay. This formula would be valid for bay lengths that make this result less than our formula $0.6fW_s(BW_s)^{1/3}$, in which case $L < 0.09fW_s^{5/3}/B^{1/3}$. Using the foregoing numbers, $L < 279$ km. This gives a length to width ratio of approximately 3 as the criterion for whether long (the present) or short (Sugimoto and Whitehead) shelf dynamics dominates. It would be hard to make L much greater since W_s is already large and B is calculated using a very large heat flux value. Moreover, B is raised to only 1/3 power. For smaller W_s, for instance, 10 km, $L < 6$ km so the bay is less wide than it is long. Thus, for shelves with aspect ratios of roughly order 1 or greater, long shelf dynamics as measured here can be expected to flux the cold water off the shelf more effectively than a geostrophic current leaning on a coast. An implication of this scaling is that if spacing of topographic features (such as canyons, banks, peninsulas) is significantly greater than shelf length, their effect on shelf to ocean transport rates might be less than the transport rates measured here. This important possibility may warrant further study.

Throughout this study the Boussinesq approximation (Spiegel and Veronis 1960) is used and temperature increase is taken to be linearly proportional to a decrease in density. Other more general constitutive relations could also be dealt with but will not be discussed here except for the effect of ice formation. Formula 13 can be altered to express forcing by brine rejection from ice formation. Consider the action on 1 cal of cooling on 1 g of seawater close to 0°C. Density of this water will change about one part in 10^4 from this cooling. If that calorie were acting on seawater that is already at its freezing temperature, about 1/80th of the water would become ice (since the latent heat of fusion of ice is close to 80 calories per gram). Assuming the ice retains 10% salinity, the seawater would increase from 35 to 35.32 psu. This would increase density of the water approximately 3×10^{-4}, which is three times greater than the increase due to thermal expansion for 1 g of water cooled by 1 cal. Thus, cooling that results in ice formation and brine rejection increases density approximately three times more than thermal cooling. This is quantified using Eq. (13) by setting buoyancy flux $B = g\beta SH/\rho L_a$, where β is salt density coefficient, S is salinity difference between ocean and ice, and L_a is latent heat of fusion of ice so that

$$g' = \frac{7.4}{h}\left(\frac{g\beta SHW_s}{\rho L_a}\right)^{2/3} + 0.6\,\frac{fW_s}{h}\left(\frac{g\beta SHW_s}{\rho L_a}\right)^{1/3}. \tag{14}$$

This can be used to predict g' for an ocean shelf whose density is increased by ice formation and brine rejection. Taking the values of H, W_s, and h used at the beginning of this section and using $\beta = 0.77$, $S = 0.03$, and $L_a = 3.3 \times 10^5$ J kg^{-1}, we get a contribution to g' from the left-hand term in the brackets of 0.012 (equivalent to a density change from temperature change of about 14°C) and from the right-hand term in the brackets of 0.022 (equivalent to a density change from temperature change of about 22°C). Thus, for the same rate of cooling, the increase in density is greater from ice rejection than it is from the lowering of temperature. The volume flux is found by modifying Eq. (1) to read

$$BA = Qg'. \tag{15}$$

Using the above values of B, A, and g', a volume flux of about 2.3×10^6 m^3 s^{-1} is predicted. These numbers are also "reasonable" for the ocean situation.

We note, however, that there is still uncertainty about some previously suggested values for the Arctic Ocean. MacDonald and Carmack (1991) show that a proposal by Aagaard et al. (1985), that the excess salt in the Canada Basin comes from the surrounding continental shelves, is not supported by oxygen, tritium, or nutrient balances. Instead deep water in that basin may be old and have little present renewal. In contrast, the possibility of active convection on the Barents Sea still seems viable.

The model by Hsu (1992, private communication) appears to have dynamics with some differences and some similarities from the cross-front exchange measured here. He has conducted a numerical study of response of the polar shelf water to dense water formation. The results are influenced by rotation, and density is removed by flux through a bottom Ekman layer similar to the density flux in the Stommel–Leetmaa shelf model. A counterpart to the front seen here is found in the model, and detailed comparison between laboratory, theory, and numerical computations may be possible in the future.

The lid used to cover the deep basin has a direct ocean counterpart where sea ice covers the deep ocean but not the shelf. This applies to candidate sites of dense water formation in the Arctic and Antarctic. In these regions, offshore winds push the ice away from the coastline and produce polynyas. We emphasize, of course, that the ice edge does not exactly lie above the edge of the shelf break as in the experiment. In the

Arctic, Martin and Cavalieri (1989), from satellite microwave data, identify polynyas on the shelves next to Svalbard, Franz Josef Land, Novaya Zemlya, and Severnaya Zemlya. In the Antarctic, Foster and Carmack (1976) showed the importance of the frontal zone that divides shelf water from offshore water in the southern Weddell Sea shelf. Bromwich and Kurz (1984) reported on the presence of a polynya and gave estimates of cooling between 500 and 800 W m^{-2} from katabatic winds in western Terra Bay in the Ross Sea. Zwally et al. (1985) also discuss the distribution and effects of polynyas and leads in the Antarctic.

It is important to keep in mind the limitations of the experimental results. Although the lid used to cover the deep basin has a direct ocean counterpart where sea ice covers the deep ocean but not the shelf, other situations have no counterpart for the lid. Can the experiments with the lid be applied to such a situation in the ocean? Recall that the lid was required because if it was absent, there would be immense offshore currents in the laboratory experiments. In the case of an ocean without ice cover, cooling happens over both deep ocean and shelf. Brocard et al. conducted experiments with cooling over both places and found little effect from the cooling over the deep region. The mixed layer offshore simply became deeper than the shelf and behaved like a fluid of constant temperature. There is no reason for us to expect the ocean behaves otherwise. In addition, section 1 shows how dynamics of deep water formation is dominated by cross-shelf exchange that produces temperature differences larger than those associated with offshore stratification. Moreover, the section shown in Fig. 2 shows that the offshore front—where most temperature change happens—is present without a lid just as it is with a lid (Fig. 5). Also, the baffled and nonbaffled measurements had very little difference. These considerations are all consistent with the notion that, although the lids were a necessary compromise to eliminate the large current in the deep basin that resulted from the cylindrical geometry, they had a minor influence on the quantitative data.

The direct application of the results to an oceanic shelf cannot be done with any more precision than this since the laboratory model omits numerous features of real shelves such as transient and uneven cooling, sloping and irregular bottom, wind stress, upstream and downstream ends to the shelf, turbulence, ice coverage in the shelf, surface waves, and offshore currents. A strongly wind-driven laboratory experiment would provide a useful comparison to the present results. Numerical studies would also be useful. The present considerations provide at best some approximate estimates for magnitudes for the real ocean. It is hoped that these quantitative results will stimulate further efforts toward direct measurement of cross-shelf exchange in the ocean.

Acknowledgments. Construction of the apparatus and valuable assistance in conducting the experiment was provided by Robert E. Frazel. Suggestions by Glen Gawarkiewicz, Dave Chapman, and an anonymous referee are gratefully acknowledged. Support was received from the Coastal Sciences Section, Code 1121 CS of the Office of Naval Research under Grant N00014-89-J-1037.

REFERENCES

Aagaard, K., L. K. Coachman, and E. C. Carmack, 1981: On the halocline of the Arctic Ocean. *Deep-Sea Res.*, **28A,** 529–545.

——, J. H. Swift, and E. C. Carmack, 1985: Thermohaline circulation in the Arctic Mediterranean Seas. *J. Geophys. Res.*, **90,** 4833–4846.

Armi, L., 1986: The hydraulics of two flowing layers with different densities. *J. Fluid Mech.*, **163,** 27–58.

Batchelor, G. K., 1967: *An Introduction to Fluid Dynamics.* Cambridge University Press, 615 pp.

Beardsley, R. C., D. C. Chapman, K. H. Brink, S. R. Ramp, and R. Schultz, 1985: The Nantucket Shoals Flux Experiment (NSFE79). Part I: A basic description of the current and temperature variability. *J. Phys. Oceanogr.*, **15,** 713–748.

Brocard, D. N., and D. R. F. Harleman, 1980: Two-layer model for shallow horizontal convective circulation. *J. Fluid Mech.*, **100,** 129–146.

——, G. H. Jirka, and D. R. F. Harleman, 1977: A model for convective circulation in side arms of cooling lakes. Ralph M. Parsons Laboratory for Water Resources and Hydrodynamics Tech. Rep. 223, Department of Civil Engineering, Massachusetts Institute of Technology.

Bromwich, D. H., and D. D. Kurz, 1984: Katabatic wind forcing of the Terra Nova Bay Polynya. *J. Geophys. Res.*, **89,** 3561–3572.

Bryden, H. L., and T. H. Kinder, 1991: Steady two-layer exchange through the Strait of Gibraltar. *Deep-Sea Res.*, **38,** s445–s463.

——, and H. M. Stommel, 1984: Limiting processes that determine basic features of the circulation in the Mediterranean Sea. *Oceanol. Acta,* 7, 289–96.

Chu, P. C., and J. C. Gascard, 1991: *Deep Convection and Deep Water Formation in the Oceans: Proc. of the Int. Monterey Colloq. on Deep Convection and Deep Water Formation in the Oceans.* Elsevier, 382 pp.

Csanady, G. T., 1976: Mean circulation in shallow seas. *J. Geophys. Res.*, **81,** 5389–5399.

Endoh, M., 1977: Formation of thermohaline front by cooling of the sea surface and inflow of the fresh water. *J. Oceanogr. Soc. Japan,* **33,** 6–15.

Farmer, D. M., and L. Armi, 1986: Maximal two-layer exchange over a sill and through the combination of a sill and contraction with barotropic flow. *J. Fluid Mech.*, **164,** 53–76.

Foster, T. D., and E. C. Carmack, 1976: Frontal zone mixing and Antarctic Bottom Water formation in the southern Weddell Sea. *Deep-Sea Res.*, **23,** 301–317.

Fultz, D., 1961: Developments in controlled experiments on larger scaled geophysical problems. *Adv. Geophys.*, **7,** 1–103.

Hide, R., and P. J. Mason, 1975: Sloping convection in a rotating fluid. *Adv. Phys.*, **24,** 47–100.

Killworth, P. D. 1974: A baroclinic model of motions on Antarctic continental shelves. *Deep-Sea Res.*, **21,** 815–837.

——, 1977: Mixing on the Weddell Sea continental slope. *Deep-Sea Res.*, **24,** 427–448.

Kowalik, Z., and J. B. Matthews, 1983: Numerical study of the water movement driven by brine rejection from nearshore Arctic ice. *J. Geophys. Res.*, **88,** 2953–2958.

Long, R. R., 1975: Calculations and density distributions in a deep, strongly stratified, two-layer estuary. *J. Fluid Mech.*, **71,** 529–40.

MacDonald, R. W., and E. C. Carmack, 1991: Age of Canada Basin deep waters: A way to estimate primary production for the Arctic Ocean. *Science,* **254,** 1348–1350.

Martin, S., and D. J. Cavalieri, 1989: Contributions of the Siberian shelf polynyas to the Arctic Ocean intermediate and deep water. *J. Geophys. Res.*, **94,** 12 725–12 738.

Midttun, L., 1985: Formation of dense bottom water in the Barents Sea. *Deep-Sea Res.*, **32,** 1233–1241.

Smith, S. D., R. D. Muench, and C. H. Pease, 1990: Polynyas and leads: An overview of physical processes and environment. *J. Geophys. Res.*, **95,** 9461–9479.

Spiegel, E., and G. Veronis, 1960: On the Boussinesq approximation for a compressible fluid. *Astrophys. J.*, **131,** 442–447.

Stommel, H., and H. G. Farmer, 1952a: Abrupt change in width in two-layer open channel flow. *J. Mar. Res.*, **11,** 205–214.

——, and H. G. Farmer, 1952b: Control of salinity of an estuary by a transition. *J. Mar. Res.*, **12,** 13–20.

——, and A. Leetmaa, 1972: The circulation on the continental shelf. *Proc. Natl. Acad. Sci.*, **69,** 3380–3384.

Sugimoto, T., and John A. Whitehead, 1983: Laboratory models of bay-type continental shelves in the winter. *J. Phys. Oceanogr.*, **13,** 1819–1828.

Swift, J. H., T. Takahashi, and H. D. Livingston, 1983: The contribution of the Greenland and Barents seas to the deep water of the Arctic Ocean. *J. Geophys. Res.*, **88,** 5981–5986.

Whitehead, J. A., Jr., 1981: Laboratory models of circulation in shallow seas. *Phil. Trans. Roy. Soc. London,* **A302,** 583–595.

——, and R. E. Frazel, 1993: A laboratory model of a cooled continental shelf. Woods Hole Oceanographic Institution Tech. Rep. 93-22, 34 pp.

——, Melvin E. Stern, Glenn R. Flierl, and Barry Klinger, 1990: Experimental observations of baroclinic eddies on a sloping bottom. *J. Geophys. Res.*, **95,** 9585–9610.

Wood, I. R., 1970: A lock exchange flow. *J. Fluid Mech.*, **42,** 671–687.

Yih, C. S., 1980: *Stratified Flows.* Academic Press, 418 pp.

Zwally, H. J., J. C. Comiso, and A. L. Gordon, 1985: Antarctic offshore leads and polynyas and oceanographic effects. Oceanology of the Antarctic Continental shelf. *Antarct. Res. Ser.*, **43,** 203–226.